Porous-Organic-Framework-Templated Nitrogen-Rich Porous Carbon as a More Proficient Electrocatalyst than Pt/C for the Electrochemical Reduction of Oxygen

ARTICLE *in* CHEMISTRY - A EUROPEAN JOURNAL · JANUARY 2013

Impact Factor: 5.73 · DOI: 10.1002/chem.201202940 · Source: PubMed

5 AUTHORS, INCLUDING:

Pradip S Pachfule
CSIR - National Chemical Laboratory, Pune
44 PUBLICATIONS **1,017** CITATIONS
SEE PROFILE

Vishal Mahesh Dhavale
Tokyo Institute of Technology
15 PUBLICATIONS **128** CITATIONS
SEE PROFILE

Sharath Kandambeth
CSIR - National Chemical Laboratory, Pune
11 PUBLICATIONS **347** CITATIONS
SEE PROFILE

Rahul Banerjee
CSIR - National Chemical Laboratory, Pune
126 PUBLICATIONS **5,853** CITATIONS
SEE PROFILE

CHEMISTRY
A EUROPEAN JOURNAL

ChemPubSoc
Europe

DOI: 10.1002/chem.201202940

Porous-Organic-Framework-Templated Nitrogen-Rich Porous Carbon as a More Proficient Electrocatalyst than Pt/C for the Electrochemical Reduction of Oxygen

Pradip Pachfule, Vishal M. Dhavale, Sharath Kandambeth, Sreekumar Kurungot,* and Rahul Banerjee*[a]

Abstract: Porous nitrogen-rich carbon (POF-C-1000) that was synthesized by using a porous organic framework (POF) as a self-sacrificing host template in a nanocasting process possessed a high degree of graphitization in an ordered structural arrangement with large domains and well-ordered arrays of carbon sheets. POF-C-1000 exhibits favorable electrocatalytic activity for the oxygen-reduction reaction (ORR) with a clear positive shift of about 40 mV in the onset potential compared to that of a traditional, commercially available Pt/C catalyst. In addition, irrespective of its moderate surface area ($785\ m^2 g^{-1}$), POF-C-1000 showed a reasonable H_2 adsorption of 1.6 wt% (77 K) and a CO_2 uptake of $3.5\ mmol\ g^{-1}$ (273 K).

Keywords: adsorption · electrochemistry · fuel cells · oxygen-reduction reaction · porous organic frameworks

Introduction

The synthesis of nanostructured porous carbon materials with different morphologies and various porosities has attracted significant attention owing to their applications in adsorption, electrochemical double-layer capacitors, lithium-ion batteries, polymer electrolyte membrane fuel cells (PEMFCs), electrocatalysts, field-effect transistors, etc.[1–6] Although several methods, like chemical-vapor deposition, laser ablation, electrical arcs, and the carbonization of polymer aerogels, have been used for their synthesis,[7–10] the nanocasting method is considered to be one of the most efficient ways to generate carbon materials with excellent porosities and a diverse range of doped functionalities.[11–13] In the nanocasting method, sacrificial solid templates, like mesoporous silicas or aluminosilicates (e.g. SBA-15, MCM-48, MSU-H), or metal–organic frameworks (MOFs) are initially mixed with suitable carbon precursors, such as cyanamide, sucrose, and furfuryl alcohol. Subsequently, the mixture is subjected to pyrolysis at high temperature, followed by the selective removal of the inorganic templates (occasionally metal atoms).[14–16] Recently, the use of carbon precursors, such as cyanamide and modified perylenes (e.g. PDI), have afforded carbon materials that possessed a high degree of graphitization and N doping.[17,18] Such graphitic carbon materials with moderate surface areas and high N content have shown excellent promise as possible replacements of the expensive platinum-based catalysts (Pt alloys, core–shell nanoparticles, etc.) in PEMFCs for the electrocatalytic oxygen-reduction reaction (ORR).[19,20]

Apart from these graphitic carbon materials with high N content, several non-Pt electrocatalysts, such as metal-nanoparticle-doped carbon materials, N-doped carbon nanotubes (CNTs), and partially unzipped multi-walled CNTs, have been investigated as replacements for the traditional Pt-based ORR catalysts.[21–26] However, metal-free N-doped carbon materials still remain good candidates for the ORR reaction, owing to their unique electronic properties, which originate from the conjugation between the graphene π system and the nitrogen lone-pair. These N-containing carbon materials also possess comparatively high ORR activity, comparable electrical conductivity, and low cost.[27,28] However, the major disadvantage of preparing these materials by using the nanocasting method is the formation of metal/metal-oxide particles or inorganic impurities after pyrolysis at high temperatures. In general, the use of mesoporous silicas, aluminosilicates, or MOFs as the host templates lead to the generation of such metal/metal-oxide impurities during pyrolysis and should be removed from the bulk carbon material to obtain a phase-pure catalyst.[13] To remove these decomposed inorganic precursors from the bulk catalyst, several additional steps, like metal leaching by acid washing, drying, and activation, need to be performed, which lead to limited yields of the products. Moreover, whilst performing these post-synthetic steps to purify the catalyst, several un-

[a] P. Pachfule,[+] V. M. Dhavale,[+] S. Kandambeth, Dr. S. Kurungot, Dr. R. Banerjee
Physical/Materials Chemistry Division
CSIR-National Chemical Laboratory
Dr. Homi Bhabha Road, Pune-411008 (India)
Fax: (+91) 20-25902636
E-mail: k.sreekumar@ncl.res.in
r.banerjee@ncl.res.in

[+] These authors contributed equally to this work.

Supporting information for this article is available on the WWW under http://dx.doi.org/10.1002/chem.201202940.

necessary impurities pierce the catalyst, which result in the poisoning of the active sites and diminution of the surface area. Furthermore, this decrease in the surface area of the catalyst leads to other complexities, such as decreases in mass transport and ion exchange, together with the limitation of the seamless access between the catalyst and the reactants. Ultimately, the overall ORR activity is significantly compromised.[29,30]

Hence, a stable porous-carbon-based catalyst that can be synthesized in a single step with all of the essential features, like suitable pore size (10–12 Å), high N-content, and channels for efficient mass transport, could be the best electrocatalyst for PEMFCs.[31] Herein, for the first time, we report a new, bulk synthesis of a N-doped graphitic carbon material as a metal-free electrocatalyst in high yield and purity. This material has been achieved by using a nanocasting method with a nitrogen-rich porous organic framework (POF) as a template and furfuryl alcohol (FA) as a carbon precursor (Scheme 1). POF (PAF-6), which contained about 41% nitrogen, was used as a self-sacrificing template.[32] Because we used this metal-free POF as a self-sacrificing host template for the synthesis of the carbon material, extremely pure carbon was achieved in high yield (about 65%) without any contamination by metallic impurities. The electrocatalytic properties of the high-nitrogen-content carbon material (POF-C-1000) were analyzed by using cyclic voltammetry (CV) and a rotating disk electrode (RDE) study. A comparative study with commercially available 20 wt% Pt/C revealed matching ORR activities for these systems. The combination of more N-doped active sites (6.23 wt%) and the ordered graphitic architecture in POF-C-1000 helped the system to attain modulated surface properties and, consequently, it validated the efficiency of N-doped carbon as a potential replacement for the traditional Pt/C catalyst in PEMFCs. The carbon material that was synthesized by using the nanocasting method at an optimized temperature (1000 °C) with moderate porosity (POF-C-1000) was characterized by TEM, Raman spectroscopy, wide-angle X-ray diffraction (XRD), X-ray photoelectron spectroscopy (XPS), energy-dispersive X-ray (EDX) analysis, and by elemental analysis. The electrocatalytic properties of the high-nitrogen-content carbon material (in the ORR) were analyzed by using CV and RDE and were compared with those of commercially available 20 wt% platinized Vulcan carbon (Pt/C).

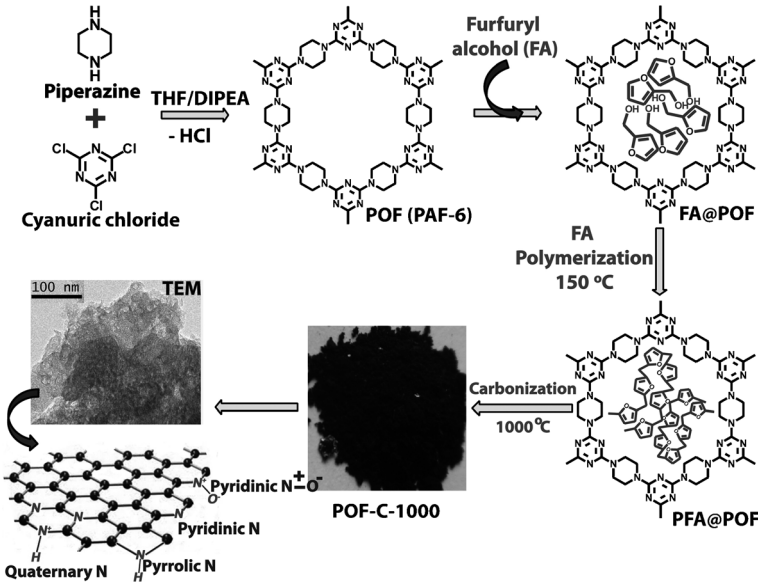

Scheme 1. Synthesis of N-rich porous carbon material POF-C-1000 from a porous organic framework (POF) at 1000 °C by using a nanocasting method.

Results and Discussion

The obtained carbon materials, POF-C-1000, POF-C-800, and POF-DC-1000, were characterized by XRD, with two broad peaks at $2\theta = 25$ and 44°, which corresponded to the graphitic (002) and (101) diffractions, respectively (Figure 1a).[33,34] From the relatively strong peak at 25° (002) in the PXRD profile of POF-C-1000, we concluded that the degree of graphitization could be higher in that material,

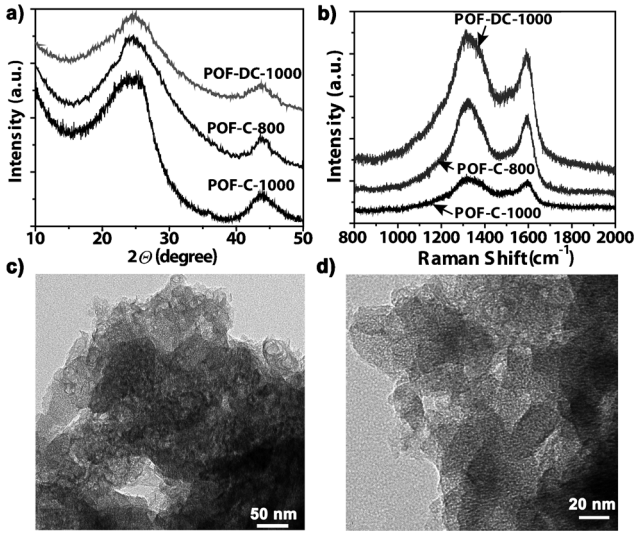

Figure 1. a) Wide-angle X-ray diffraction patterns for the carbon atoms, which show peaks for the (002) and (101) diffractions planes. b) Raman spectra of POF-C-1000, POF-C-800, and POF-DC-1000, which show their corresponding D and G bands. c) TEM image of bulk POF-C-1000, which shows an ordered structural arrangement and pore channels. d) TEM image of bulk POF-C-1000, which shows ordered domains with well-ordered arrays of carbon sheets.

thereby leading to the exposure of a higher concentration of parallel single layers than in the other samples.[35] Furthermore, Raman spectroscopy of these materials showed broad peaks at about 1345 and 1590 cm^{-1}, which corresponded to the D and G bands, respectively (Figure 1b).[34,35] The relative intensity (I_D/I_G) ratios for POF-C-1000, POF-C-800, and POF-DC-1000 are 1.04, 1.13, and 1.15, respectively (see the Supporting Information, Figures S19, S25, and S30). POF-C-1000, which was obtained at 1000 °C, showed more graphitization than the other synthesized carbon materials, which signified the effects of FA loading and pyrolysis temperature. The ordered structural arrangement of POF-C-1000, with large domains and well-ordered arrays of the carbon sheets and pore channels, has been observed by using TEM (Figure 1c). High-resolution TEM (HRTEM) images indicated the formation of crystalline frameworks and the orientation of the graphite layers, thus showing a highly ordered porous structure for POF-C-1000 (Figure 1d). On the other hand, the TEM images of POF-C-800 and POF-DC-1000 showed a less-ordered structural arrangement, with a comparatively compact morphology, which indicated lower porosity and lower degrees of graphitization (see the Supporting Information, Sections S3–S5). Centered and slightly asymmetric XPS C 1s spectra for POF-C-1000 at 285 eV are shown in the Supporting Information, Figure S36. Moreover, its narrow full width at half maximum (FWHM) suggests increased graphitic character and good agreement with the Raman analysis.[36–38] The complex XPS N 1s spectra could be deconvoluted (Figure 2a) into four sub-peaks, which were due to spin-orbit coupling. These four N sub-peaks are assigned to the pyridinic N, pyrrolic N, quaternary N, and pyridine N-oxide atoms at 398.4, 399.7, 401.3, and 402.8 eV, respectively.[38] The calculated nitrogen content from the XPS data (5.57 wt%) showed close resemblance to that from the EDX data (6.80 wt%) and from elemental analysis (6.23 wt%), with high pyridinic N content (about 3 at.%; see the Supporting Information, Section S6). Elemental analysis and EDX spectroscopy of the carbon materials revealed the absence of metallic impurities with high N content, which confirmed the importance of this synthetic procedure for in situ N doping into the carbon matrix (see the Supporting Information, Figures S20, S26, and S31).

The N_2-adsorption isotherms of POF-C-1000, POF-C-800, and POF-DC-1000 show typical type-I isotherms without any hysteresis loop. The Brunauer–Emmett–Teller (BET) and Langmuir surface areas for POF-C-1000 are 785 and 1079 $m^2 g^{-1}$, respectively (Figure 2b). POF-C-1000 shows an average pore size and total pore volume of 17.9 Å and 0.701 $cc\,g^{-1}$, respectively. Likewise, the BET surface areas of POF-C-800 and POF-DC-1000, within the same relative-pressure range, are 335 and 100 $m^2 g^{-1}$, respectively, thus confirming the importance of FA loading and temperature during the synthesis for acquiring high surface areas (Table 1). Because these carbon materials had moderate surface areas and high N content, we studied their H_2 (77 K) and CO_2 adsorptions

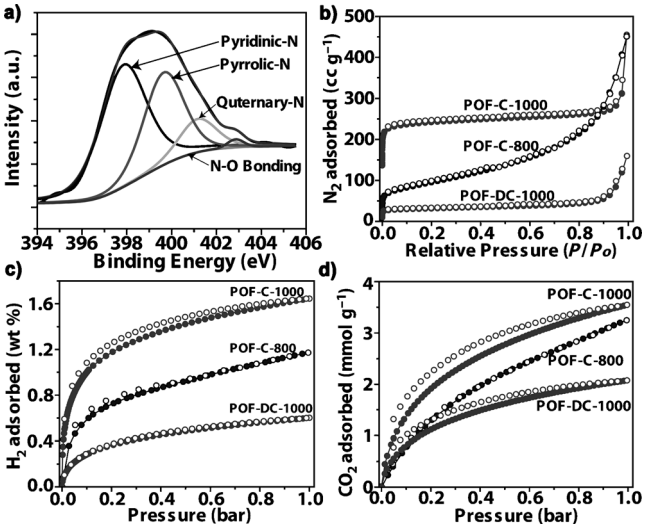

Figure 2. a) The complex N 1s XPS spectra of POF-C-1000, which shows four types of nitrogen atoms in the bulk carbon matrix. b) N_2-adsorption isotherms for POF-C-1000, POF-C-800, and POF-DC-1000. c) H_2-adsorption isotherms for POF-C-1000, POF-C-800, and POF-DC-1000 at 77 K and 1 bar pressure. d) CO_2-adsorption isotherms for POF-C-1000, POF-C-800, and POF-DC-1000 at 273 K and pressures below 1 bar.

(273 K and 298 K) at 1 atm pressure. Typical type-I isotherms without any hysteresis loop confirmed the reversible uptake of H_2 and CO_2 in POF-C-1000, POF-C-800, and POF-DC-1000 (Figure 2c,d). As shown in Figure 2c, POF-C-1000 showed a H_2 uptake of 1.64 wt%, whereas POF-C-800 and POF-DC-1000 showed H_2 uptake of 1.17 and 0.60 wt%, respectively. The higher H_2 uptake in the case of POF-C-1000 compared to POF-C-800 and POF-DC-1000 was well-justified because it had a high surface area with ordered pore channels. The CO_2-adsorption isotherms (at 273 and 298 K) for POF-C-1000 showed uptake of 3.54 and 2.76 mmol g^{-1}, respectively (see the Supporting Information, Figure S23). The CO_2-adsorption isotherms at 273 K for POF-C-800 and POF-DC-1000 showed relatively lower CO_2 uptake of 3.24 and 2.07 mmol g^{-1}, respectively (Figure 2d). The surface area of POF-C-1000 is comparable to that of other carbon materials, like NPC_{800} (1141 $m^2 g^{-1}$)[39] and 5C (988 $m^2 g^{-1}$),[41] and is higher than those of Z-600 (24 $m^2 g^{-1}$), Z-700 (520 $m^2 g^{-1}$), Z-800 (720 $m^2 g^{-1}$),[40] MAC (384 $m^2 g^{-1}$),[42] Al-PCP-FA1 (263 $m^2 g^{-1}$), and Al-PCP-FA2 (513 $m^2 g^{-1}$),[43] which were synthesized by using MOFs as templates. The CO_2 uptake of POF-C-1000 at room temper-

Table 1. Summary of surface area, average pore size, total pore volume, H_2 and CO_2 uptake for POF-C-1000, POF-C-800, and POF-DC-1000.

	BET surface area [$m^2 g^{-1}$]	Total pore volume [$cc\,g^{-1}$]	H_2 uptake [wt%][a]	CO_2 uptake [mmol g^{-1}][b]
POF-C-1000	785	0.701	1.64	3.54
POF-C-800	335	0.564	1.17	3.24
POF-DC-1000	100	0.246	0.60	2.07
POF (PAF-6)	177	0.205	0.69	1.81

[a] H_2-uptake isotherms were collected at 77 K. [b] CO_2-uptake isotherms were collected at 273 K.

ature (298 K) and under atmospheric pressure is comparable to that of well-known commercial carbon materials, such as MAXSORB (1.98 mmol g^{-1}) and Norit RB2 (3.11 mmol g^{-1}), zeolites, such as 13X zeolite (3.50 mmol g^{-1}),[44] carbon molecular sieves, such as VR-5 (4.54 mmol g^{-1}) and VR-93 (4.77 mmol g^{-1}),[46] and some MOFs[44,45] (see the Supporting Information, Table S1). The most important and notable thing about POF-C-1000 is that its H_2- and CO_2-uptake properties are twice that of its template POF material (H_2: 0.69 wt%, CO_2: 1.81 mmol g^{-1}; see the Supporting Information, Figures S8 and S9).

As mentioned earlier, the carbon materials that have a high degree of graphitization with N-doping have shown very promising applications as substitutes for the traditional and costly Pt catalyst in the electrocatalytic ORR. Carbon materials POF-C-1000 and POF-C-800 show electrical conductivities (see the Supporting Information, Figure S35) of about 0.54 S cm^{-1}, which are close to that of Vulcan XC-72 (about 0.55 S cm^{-1}), owing to the variation in the degree of graphitization with N content. Furthermore, we have investigated the electrochemical ORR activity of these systems to understand the viability of using them as metal-free electrocatalysts in PEMFCs instead of Pt/C. From the XPS analysis of POF-C-1000, it is clear that the bulk catalyst contains four types N atoms, that is, pyridinic N, pyrrolic N, quaternary N, and pyridine N-oxide atoms (Figure 2a). Of these, the pyridinic N and pyrrolic N atoms are the most-active sites for facilitating the ORR.[38] It has been documented that the pyridinic N atom donates one π electron to the aromatic system. The lone pair of electrons on the pyridinic N atom in the plane of the carbon matrix leads to an increase in the electron-donating properties of the neighboring carbon atoms. This charge dislocation assists in the weakening of the O–O bond through bonding between the oxygen atoms and the active sites, which, subsequently, leads to the reduction of oxygen. Screening of the materials for judging their ORR activity was achieved by using CV in a nitrogen- and oxygen-saturated 0.1 M aqueous solutions of KOH as the electrolyte at a scan rate of 50 mV s^{-1} (see the Supporting Information, Figures S37 and S39). All of the catalysts were compared with 20 wt% Pt/C. In all of the cases, 20 μg of the catalyst was loaded onto a glassy carbon electrode (diameter: 3 mm). The CV scans were recorded within a potential window of −1 to 0.3 V (versus Hg/HgO). In the nitrogen-saturated 0.1 M KOH electrolyte, all three carbon materials showed similar pseudo-capacitive behavior (see the Supporting Information, Figure S38). On the contrary, when the electrolyte had been saturated with oxygen, the catalysts started showing the oxygen-reduction process (Figure 3a). In fact, POF-C-1000 exhibited the highest electrocatalytic activity for the ORR, as reflected from its higher positive shift in the onset potential and higher cathodic current density of 5.3 mA cm^{-2} than POF-C-800 (2.7 mA cm^{-2}) and POF-DC-1000 (2 mA cm^{-2}) at −0.2 V. Most importantly, as shown in Figure 3b, the onset potential of POF-C-1000

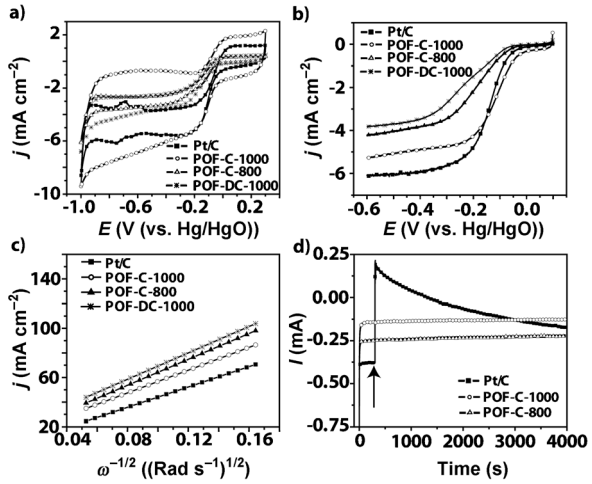

Figure 3. a) Comparative CVs of Pt/C, POF-C-1000, POF-C-800, and POF-DC-1000 in oxygen-saturated 0.1 M KOH at a scan rate of 50 mV s^{-1}. b) Comparative linear-sweep voltammograms in 0.1 M KOH under oxygen bubbling at a scan rate of 10 mV s^{-1} and an electrode-rotation speed of 1600 rpm. c) Comparative K–L plots at −0.44 V. d) Comparative chronoamperometric responses of Pt/C, POF-C-1000, and POF-C-800 in 0.1 M KOH and 3 M MeOH solution at −0.16 V. The arrow shows the addition of MeOH at 300 s.

was about 40 mV higher than that of Pt/C. Furthermore, the ORR kinetics for the as-synthesized porous carbon materials and Pt/C have been investigated by hydrodynamic linear-sweep voltametry (LSV) in oxygen-saturated 0.1 M KOH electrolyte at a scan rate of 10 mV s^{-1} by using a RDE setup (Figure 3b and the Supporting Information, S40). From the LSVs of POF-C-1000, POF-C-800, POF-DC-1000, and Pt/C, the limiting current density was found to be higher for POF-C-1000 (5.2 mA cm^{-2}) compared to POF-C-800 (4.2 mA cm^{-2}) and POF-DC-1000 (3.8 mA cm^{-2}), but less than that of Pt/C (6.09 mA cm^{-2}). This higher limiting current in POF-C-1000 could be attributed to its well-ordered graphitization and porous nature, which provide proper channels for mass diffusion (Table 2).

The kinetic parameters of the ORR can be analyzed on the basis of the Koutecky–Levich (K–L) equation and K–L plots at different potentials (see the Supporting Information, Figure S41) by incorporating the corresponding values of the parameters into the equation. A brief discussion on the K–L equation and the analysis of the plots is given in the

Table 2. Summary of the electrochemical properties of POF-C-1000, POF-C-800, POF-DC-1000, and Pt/C in 0.1 M KOH electrolyte with a carbon loading of 20 μg and a potential window of 1.3 V.

	Onset potential [mV] (versus Hg/HgO)[a]	Limiting current density [mA cm^{-2}][b]	j_k [mA cm^{-2}] (at −0.44 V)	n (no. of electron transfers at −0.44 V)
POF-C-1000	−93.11	5.24	20	3.75
POF-C-800	−77.87	4.21	17	3.53
POF-DC-1000	−98.57	3.85	12	3.46
Pt/C (20 wt% Pt)	−53.03	6.09	75	3.90

[a] Onset potential was calculated at a current density of −0.3737 mA cm^{-2}. [b] Limiting current density was calculated at a voltage of −0.6 V.

Supporting Information, Section S6. The corresponding K–L plots (j^{-1} versus $\omega^{-1/2}$, where j is the current density and ω is the angular rotation speed of the electrode) at various electrode potentials display good linearity (Figure 3c); the slopes remain approximately constant over the potential range of −0.6 to −0.3 V, which suggest that the electron-transfer numbers for ORR at different electrode potentials are similar. Linearity and parallel behavior of the plots are usually taken as an indication of first-order reaction kinetics with respect to the concentration of the dissolved oxygen. The number of transferred electrons during the ORR is estimated to be about 4, which indicates that all of the catalysts proceed through a similar mechanism, that is, the direct formation of the hydroxide ion. Moreover, the calculated kinetic-current densities (j_k) at −0.44 V (versus Hg/HgO) from the K–L plots are in the order Pt/C (75 mA cm^{-2}) > POF-C-1000 (20 mA cm^{-2}) > POF-C-800 (17 mA cm^{-2}) > POF-DC-1000 (12.8 mA cm^{-2}). The obtained j_k values for these catalysts are much higher than those reported in the literature for N-doped CNTs in acid medium (3.54 mA cm^{-2} at −0.1 V versus Ag/AgCl) and those of vertically aligned CNTs (4.24 mA cm^{-2} at −0.3 V versus SCE).[47,48] Of the three synthesized carbon electrocatalysts, the j_k value of POF-C-1000 is twice as high as that of POF-DC-1000. However, the calculated n values are almost same in all cases (about 4), which indicates the major influence of FA and the pyrolysis temperature, which lead to graphitization and controlled porosity in POF-C-1000. Notably, even though POF-C-1000 has a lower j_k value than Pt/C, it has an about 40 mV gain in the positive onset potential, as revealed from the LSVs, which is more significant than that of any other N-rich carbon catalyst.

Furthermore, the synthesized catalyst has been tested for MeOH crossover and stability in the ORR by a chronoamperometric study. Figure 3d shows the comparative chronoamperometric responses of Pt/C, POF-C-1000, and POF-C-800 in a 0.1 M solution of KOH electrolyte with 3 M MeOH at −0.16 V for 4000 s. The arrow shows the addition of MeOH (200 μL) at 300 s after the start of the run. The amperometric responses for POF-C-1000 and POF-C-800 remain unchanged, even after the addition of MeOH. In contrast, a drastic change in the current, owing to the oxidation of MeOH at the addition point, can be observed for Pt/C. These results validate the high fuel selectivity of these N-doped catalysts compared to Pt/C. Taking into account the similar elemental compositions of the three POF-derived carbon catalysts, the gain in onset potential during the ORR of POF-C-1000 and no change in the current after the addition of MeOH can be attributed to the effect of the porous structure on the diffusion rate of the electrolyte and the exposed active sites, which are closely related to its high BET surface area (785 m^2 g^{-1}). Moreover, XPS analysis showed the presence of pyridinic N as well as pyrrolic N peaks, which were more likely to be active towards the ORR, as confirmed by the electrochemical study. These results clearly highlight the effects of carbonization temperature and the carbon precursor (FA), which mainly control the graphitization and porosity, respectively, on the obtained carbon materials.

Conclusion

In summary, we have developed a new route for the synthesis of porous, N-rich carbon materials (about 6 wt%) with a high degree of graphitization by using a nanocasting method in which POF and FA were used as a self-sacrificing host template and a carbon precursor, respectively. The obtained carbon material (POF-C-1000) possesses high N content and moderate porosity (785 m^2 g^{-1}) and displays a higher onset potential (by about 40 mV) for oxygen reduction than the commercially available Pt/C catalyst. The ORR proceeds through a mechanism that involves about four electron-transfer steps and shows first-order reaction kinetics with respect to the concentration of the dissolved oxygen. Moreover, these carbon materials show high H_2- and CO_2-uptake capacity, although they only have moderate porosity. The H_2- and CO_2-uptake properties of POF-C-1000, along with its performance in the ORR, indicate the multifunctional nature of this carbon material. We believe that this strategy for the synthesis of carbon materials by using POFs can be further extended to procure carbon materials with excellent ORR activity and fuel selectivity for future applications in the field of fuel cells, supercapacitors, sensors, and batteries.

Experimental Section

Materials: For the synthesis of POF, cyanuric chloride, THF, and piperazine were purchased from Sigma–Aldrich. Furfuryl alcohol and *N,N*-diisopropyl ethylamine were purchased from Avra Synthesis. All of the starting materials were used without further purification. THF was distilled before use to remove any trace impurities and moisture. HPLC-grade CH_2Cl_2 and MeOH for the solvent exchange were purchased from Sigma–Aldrich and used as received. All of the experimental operations in the synthesis of POF were performed in air. An argon atmosphere was used for the polymerization of furfuryl alcohol, as well as for the synthesis of the porous carbon materials.

Synthesis of POF-C-1000: A typical synthesis of the POF-derived carbon material is shown in Scheme 1. Highly pure 2D POF (PAF-6, 0.50 g),[32] which was synthesized according to a literature procedure (see the Supporting Information, Section S2), was stirred with FA (5.0 g, 0.05 mmol) at RT under a N_2 atmosphere for 24 h so as to fill the pores with FA (FA@POF). Next, whilst maintaining a continuous flow of N_2, the whole FA@POF composite mixture was heated at 90 °C for 24 h. To obtain the polymerization of FA inside the pores (PFA@POF), the composite mixture of FA@POF was heated at 150 °C for 8 h under a N_2 atmosphere. To facilitate the removal of FA and PFA molecules that had adsorbed onto the POF surface, the PFA@POF composite was washed with absolute EtOH (99.99%) a few times. Because a higher loading of FA inside the template leads to both a higher yield and higher porosity of the resulting carbon material, to achieve a higher loading of FA inside the POF pores, the same composite (PFA@POF) was subjected to the impregnation of FA, followed by the polymerization process, one more time according to the aforementioned procedure. The PFA@POF composite was carefully filtered and washed with EtOH several times to remove the FA that had physically adsorbed onto the surface. The increase in the weight of POF from bare POF (0.50 gm) to PFA@POF (0.98 g) was probably due to the quantitative loading of FA/PFA onto the POF surface or inside the

pores. The roughly calculated differential loading of PFA was 96%, which reflected the higher incorporation of PFA inside the pores of the bare POF. Accordingly, the obtained PFA@POF was subjected to carbonization at 1000°C for 3 h at a heating rate of 5°C min^{-1} under an argon atmosphere in a silicon container (Scheme 1). Finally, after the pyrolysis of PFA@POF, the carbon material (POF-C-1000) was collected and activated at 250°C for 24 h to remove any trapped water molecules before analysis.

Synthesis of POF-C-800: The effect of temperature on the morphology and porosity of the resulting carbon material was determined by using a carbonization temperature of 800°C for the conversion of PFA@POF into POF-C-800. The synthesis of POF-C-800 was performed according to the same procedure as for POF-C-1000, except that the carbonization temperature was 800°C. Specifically, the PFA@POF material that was obtained by using the aforementioned procedure was subjected to carbonization at 800°C for 3 h at a heating rate of 5°C min^{-1} under an argon atmosphere in a silicon container. Finally, after the pyrolysis of PFA@POF, the obtained carbon material (POF-C-800) was collected and activated at 250°C for 24 h to remove any trapped water molecules before analysis.

Synthesis of POF-DC-1000: To determine the effect of the FA template on the yield, morphology, and porosity of the resulting carbon material, POF-DC-1000 was synthesized at 1000°C by the direct carbonization (DC) of the evacuated POF, without the loading of any template, under an argon atmosphere. The synthesis of POF-DC-1000 was performed by the direct carbonization of POF (PAF-6) at 1000°C for 3 h at a heating rate of 5°C min^{-1} under an argon atmosphere in a silicon container, without the incorporation of a carbon precursor. Finally, after the pyrolysis of PFA, the obtained carbon material (POF-DC-1000) was collected and activated at 250°C for 24 h to remove any trapped water molecules before analysis.

PXRD and Raman, XPS, and solid-state ^{13}C NMR spectroscopy: X-ray diffraction was performed on a PANalytical X′PERT PRO instrument by using iron-filtered $Cu_{K\alpha}$ radiation ($\lambda = 1.5406$ Å) in the range $2\theta = 5$–50° with a step size of 0.02° and $t = 0.3$ s per step.

Raman spectroscopy was performed on a HR 800 Raman spectrophotometer (Jobin Yvon-Horiba, France) by using monochromatic radiation from a He-Ne laser (632.8 nm) that operated at 20 mW. The experiments were repeated several times to verify the consistency of the data.

X-ray photoelectron spectroscopy (XPS) was performed on a VG Micro Tech ESCA 3000 instrument at a pressure of $> 1 \times 10^{-9}$ Torr (pass energy: 50 eV, electron take-off angle: 60°, overall resolution: about 0.1 eV).

Solid-state NMR spectroscopy was performed on a Bruker Avance 300 spectrometer (^{13}C: 75.5 MHz) that was equipped with 4 mm double resonance MAS probes and operated at a static field of 7.04 T. Samples in the form of fine powder were packed in a 4 mm O.D. zirconia rotor under a nitrogen atmosphere and spun at a spinning speed of 8 kHz for the ^{13}C CPMAS experiments. Chemical shifts were referenced to TMS by using adamantane as an external standard.

Gas adsorption and pore-size distribution: Low-pressure volumetric H_2- and N_2-adsorption measurements were performed on an Autosorb-iQ automatic volumetric instrument at 77 K (maintained by using a liquid-nitrogen bath) with pressures in the range 0–760 Torr. CO_2-adsorption measurements were performed at RT (298 K) and at 273 K, within the same pressure range, on a Quantachrome Quadrasorb automatic volumetric instrument. For all of the adsorption measurements, ultrahigh-purity H_2 was obtained by using calcium-aluminosilicate adsorbents to remove any trace amounts of water and other impurities before its introduction into the system. For the gas-adsorption studies of POF, the solvent-exchanged sample was dried overnight at RT under a dynamic vacuum ($< 10^{-3}$ Torr), followed by heating at 100°C for 12 h and 120°C for 12 h under a dynamic vacuum. The completely dried samples (0.050 gm) were loaded into the sample cells for the gas-adsorption study. The sample that was prepared by the inclusion of PFA into POF (PFA@POF) was loaded for the N_2-adsorption study as synthesized. For the gas-uptake studies of POF-C-1000, POF-C-800, and POF-DC-1000, the samples were activated at 250°C for 24 h to remove any trapped water molecules before analysis. For the gas-uptake study of Pt/C (Pt carbon black), the same procedure was followed to activate the sample. The pore-distributions plots were calculated by using quenched-solid density functional theory (QSDFT) and density functional theory (DFT) methods by using the nitrogen-adsorption isotherms that were obtained at 77 K and at 1 atm pressure.

Electrode preparation: Electrochemical properties were investigated by cyclic voltammetry (CV) and by linear-sweep voltammetry (LSV) on a BioLogic Science Instrument in a conventional three-electrode cell with Hg/HgO as the reference electrode and Pt foil as the counter electrode. Before the preparation of the working electrode (WE), the glassy carbon electrode (GCE, surface area: 0.07065 cm^2) was polished on 0.3 μm alumina powder and was sonicated several times alternately in de-ionized water and EtOH (2 min in each) and dried under a lamp. The catalyst slurry was made by sonicating the catalyst (5 mg) in a 3:2 EtOH/water mixture (1 mL) and was drop-coated onto a previously polished GCE to achieve a constant loading of 20 mg in all cases to minimize the internal diffusion limitation owing to the thickness of the electrode. A solution of Nafion (0.01 wt%, 2 mL) was applied over the whole surface of the electrode to afford a uniformly thin film. The electrode was dried in air and was used as the working electrode for all further electrochemical studies. An aqueous solution of 0.1 M KOH, which had been de-aerated with N_2, was used as an electrolyte for the normal CV and RDE studies. For the MeOH crossover study, a 3 M solution of MeOH (200 μL) was used as the electrolyte, with 0.1 M KOH as the supporting electrolyte. Plots were normalized by dividing the measured currents by the geometrical area of the working electrode.

Acknowledgements

P.P. and V.M.D. acknowledge the CSIR for a Senior Research Fellowship and S.K. acknowledges the CSIR for a Junior Research Fellowship. R.B. and S.K. acknowledge the XIth Five Year Plan Project of the CSIR (NWP0022 and NWP0021). Financial assistance from the DST (SR/S1/IC-22/2009) and the BRNS (2011/37C/44/BRNS) is acknowledged.

[1] A. C. Dillon, K. M. Jones, T. A. Bekkedahl, C. H. Kiang, D. S. Bethune, M. J. Heben, *Nature* **1997**, *386*, 377–379.
[2] R. Ryoo, S. H. Joo, M. Kruk, M. Jaroniec, *Adv. Mater.* **2001**, *13*, 677–681.
[3] M. Winter, R. J. Brodd, *Chem. Rev.* **2004**, *104*, 4245–4269.
[4] J. Wu, W. Pisula, K. Mullen, *Chem. Rev.* **2007**, *107*, 718–747.
[5] R. J. White, V. Budarin, R. Luque, J. H. Clark, D. J. Macquarrie, *Chem. Soc. Rev.* **2009**, *38*, 3401–3418.
[6] K. Yang, B. Xing, *Chem. Rev.* **2010**, *110*, 5989–6008.
[7] J.-S. Yu, S. Kang, S. B. Yoon, G. Chai, *J. Am. Chem. Soc.* **2002**, *124*, 9382–9383.
[8] D. J. Cott, N. Petkov, M. A. Morris, B. Platschek, T. Bein, J. D. Holmes, *J. Am. Chem. Soc.* **2006**, *128*, 3920–3921.
[9] C. Liang, Z. Li, S. Dai, *Angew. Chem.* **2008**, *120*, 3754–3776; *Angew. Chem. Int. Ed.* **2008**, *47*, 3696–3717.
[10] H. Wang, Q. Gao, J. Hu, *J. Am. Chem. Soc.* **2009**, *131*, 7016–7022.
[11] A.-H. Lu, F. Schüth, *Adv. Mater.* **2006**, *18*, 1793–1805.
[12] Y. Xia, Z. Yang, R. Mokaya, *Nanoscale* **2010**, *2*, 639–659.
[13] A.-H. Lu, D. Zhao, Y. Wan in *Nanocasting: A Versatile Strategy for Creating Nanostructured Porous Materials*, RSC Publishing, Cambridge, **2009**.
[14] J. Lee, S. Han, T. Hyeon, *J. Mater. Chem.* **2004**, *14*, 478–486.
[15] C. Guan, K. Wang, C. Yang, X. S. Zhao, *Microporous Mesoporous Mater.* **2009**, *118*, 503–507.
[16] H.-L. Jiang, Q. Xu, *Chem. Commun.* **2011**, *47*, 3351–3370.
[17] F. Goettmann, A. Fischer, M. Antonietti, A. Thomas, *Angew. Chem.* **2006**, *118*, 4579–4583; *Angew. Chem. Int. Ed.* **2006**, *45*, 4467–4471.
[18] R. Liu, D. Wu, X. Feng, K. Mullen, *Angew. Chem.* **2010**, *122*, 2619–2623; *Angew. Chem. Int. Ed.* **2010**, *49*, 2565–2569.
[19] M. K. Debe, *Nature* **2012**, *486*, 43–51.

[20] Y.-J. Wang, D. P. Wilkinson, J. Zhang, *Chem. Rev.* **2011**, *111*, 7625–7651.
[21] K. Gong, F. Du, Z. Xia, M. Durstock, L. Dai, *Science* **2009**, *323*, 760–764.
[22] D. Wei, Y. Liu, Y. Wang, H. Zhang, L. Huang, G. Yu, *Nano Lett.* **2009**, *9*, 1752–1758.
[23] Z. Wang, R. Jia, J. Zheng, J. Zhao, L. Li, J. Song, Z. Zhu, *ACS Nano* **2011**, *5*, 1677–1684.
[24] Z.-S. Wu, S. Yang, Y. Sun, K. Parvez, X. Feng, K. Mullen, *J. Am. Chem. Soc.* **2012**, *134*, 9082–9085.
[25] J. Liang, Y. Zheng, J. Chen, J. Liu, D. Hulicova-Jurcakova, M. Jaroniec, S. Z. Qiao, *Angew. Chem. Int. Ed.* **2012**, *51*, 3892–3896.
[26] Y. Li, W. Zhou, H. Wang, L. Xie, Y. Liang, F. Wei, J.-C. Idrobo, S. J. Pennycook, H. Dai, *Nat. Nanotechnol.* **2012**, *7*, 394–400.
[27] M. Tiemann, *Chem. Mater.* **2008**, *20*, 961–971.
[28] K. E. Shopsowitz, W. Y. Hamad, M. J. MacLachlan, *Angew. Chem.* **2011**, *123*, 11183–11187; *Angew. Chem. Int. Ed.* **2011**, *50*, 10991–10995.
[29] L. Birry, J. H. Zagal, J.-P. Dodelet, *Electrochem. Commun.* **2010**, *12*, 628–631.
[30] M. Chen, C. Du, J. Zhang, P. Wang, T. Zhu, *J. Power Sources* **2011**, *196*, 620–626.
[31] J. Lee, J. Kim, T. Hyeon, *Adv. Mater.* **2006**, *18*, 2073–2094.
[32] H. Zhao, Z. Jin, H. Su, X. Jing, F. Sun, G. Zhu, *Chem. Commun.* **2011**, *47*, 6389–6391.
[33] N. Bozovic, I. Bozovic, J. Misewich, *Nano Lett.* **2008**, *8*, 4477–4482.
[34] C. N. R. Rao, K. Biswas, K. S. Subrahmanyam, A. Govindaraj, *J. Mater. Chem.* **2009**, *19*, 2457–2469.
[35] M. S. Dresselhaus, A. Jorio, M. Hofmann, G. Dresselhaus, R. Saito, *Nano Lett.* **2010**, *10*, 751–758.
[36] T. I. T. Okpalugo, P. Papakonstantinou, H. Murphy, J. McLaughlin, N. M. D. Brown, *Carbon* **2005**, *43*, 153–161.
[37] C. Morant, J. Andrey, P. Prieto, D. Mendiola, J. M. Sanz, E. Elizalde, *Phys. Status Solidi A* **2006**, *203*, 1069–1075.
[38] J. F. Moulder, *Handbook of X-ray Photoelectron Spectroscopy: A Reference Book of Standard Spectra for Identification and Interpretation of XPS Data*, Physical Electronics, Eden Prairie, **1995**.
[39] B. Liu, H. Shioyama, H.-L. Jiang, X. B. Zhang, Q. Xu, *Carbon* **2010**, *48*, 456–463.
[40] W. Chaikittisilp, M. Hu, H. Wang, H.-S. Huang, T. Fujita, K. C.-W. Wu, L.-C. Chen, Y. Yamauchi, K. Ariga, *Chem. Commun.* **2012**, *48*, 7259–7261.
[41] S. Lim, K. Suh, Y. Kim, M. Yoon, H. Park, D. N. Dybtsev, K. Kim, *Chem. Commun.* **2012**, *48*, 7447–7449.
[42] J. Hu, H. Wang, Q. Gao, H. Guo, *Carbon* **2010**, *48*, 3599–3606.
[43] L. Radhakrishnan, J. Reboul, S. Furukawa, P. Srinivasu, S. Kitagawa, Y. Yamauchi, *Chem. Mater.* **2011**, *23*, 1225–1231.
[44] A. R. Millward, O. M. Yaghi, *J. Am. Chem. Soc.* **2005**, *127*, 17998–17999.
[45] R. Banerjee, H. Furukawa, D. Britt, C. Knobler, M. O'Keeffe, O. M. Yaghi, *J. Am. Chem. Soc.* **2009**, *131*, 3875–3877.
[46] J. Silvestre-Albero, A. Wahby, A. Sepúlveda-Escribano, M. Martínez-Escandell, K. Kaneko, F. Rodríguez-Reinoso, *Chem. Commun.* **2011**, *47*, 6840–6842.
[47] D. Yu, Q. Zhang, L. Dai, *J. Am. Chem. Soc.* **2010**, *132*, 15127–15129.
[48] S. Wang, E. Iyyamperumal, A. Roy, Y. Xue, D. Yu, L. Dai, *Angew. Chem.* **2011**, *123*, 11960–11964; *Angew. Chem. Int. Ed.* **2011**, *50*, 11756–11760.

Received: August 17, 2012
Published online: November 30, 2012

